Rational Design of Cyclopenta[2,1-b;3,4-b′] dithiophene-bridged Hole Transporting Materials for Highly Efficient and Stable Perovskite Solar Cells

Yan-Duo Lin[+],*[b] Kun-Mu Lee[+],*[c, d, e] Bo-Yu Ke,[a] Kai-Shiang Chen,[f] Hao-Chien Cheng,[f] Wei-Juih Lin,[f] Sheng Hsiung Chang,[g] Chun-Guey Wu,*[h, i] Ming-Chung Kuo,[a] Hsin-Cheng Chung,[b] Chien-Chun Chou,[b] Heng-Yu Chen,[b] Kang-Ling Liau,[h] Tahsin J. Chow,*[a, j] and Shih-Sheng Sun*[a]

A series of small-molecule-based hole-transporting materials (HTMs) featuring a 4*H*-cyclopenta[2,1-b:3,4-b′]dithiophene as the central core with triphenylamine- and carbazole-based side groups was synthesized and evaluated for perovskite solar cells. The correlations of the chemical structure of the HTMs on the photovoltaic performance were explored through different combinations of the central π-bridge moieties. The optical and electrochemical properties, energy levels, and hole mobility were systematically investigated, revealing the significant influence of the central core planarity and packing structure on their photovoltaic performance. The optimized device based on **CT1** exhibited a PCE (power conversion efficiency) of 17.71 % with a device architecture of FTO/TiO_2 compact layer/TiO_2 mesoporous/$CH_3NH_3PbI_3$/HTM/MoO_3/Ag, which was found to be on par with that of a cell fabricated based on state-of-the-art spiro-OMeTAD (16.97 %) as HTM. Moreover, stability assessment showed an improved stability for CPDT-based HTMs in comparison with spiro-OMeTAD over 1300 h.

Introduction

Photovoltaic cells are one of the most promising alternatives for energy conversion. Since the first report was documented by Miyasaka and co-workers,[1] organic-inorganic hybrid halide perovskite solar cells (PSCs) have attracted great attention owning to their outstanding properties including high extinction coefficients, long charge carrier diffusion length, and high carrier mobility.[2–4] To date, the power conversion efficiency (PCE) for PSCs over 20 % have been reached[3–8] and this was achieved using 2,2′,7,7′-tetrakis-(*N*,*N*-di-*p*-methoxyphenyl-amine)-9,9′-spirobifluorene (spiro-OMeTAD) as a hole transporting material (HTM) despite its multiplex synthetic approach and purification.[9] In this respect, it is important to develop cost-effective HTMs for further improving PCE. Recently, various types of HTMs based on small organic molecules, polymers and inorganic salts have been reported.[10–15] However, small-molecule-based HTMs are considered to be more valuable over polymer materials because of their facile purification, high purity and smaller batch-to-batch variations in the molecular weights. A wide number of reports on high efficiencies of PSCs with organic molecule-based HTMs has been developed such as spiro-type,[9,16,17] truxene,[18] triazatruxene,[19] azulene,[20] benzotrithiophene,[21] carbazole-,[22] anthracene-,[23] and bimesitylenes-based derivatives.[24] Despite tremendous efforts have been made to develop small molecule-based HTMs for PSCs, there were few reports to elucidate the correlations between the chemical structures of HTMs and the corresponding roles played in the photovoltaic devices.[25–27]

Fused-thiophene based organic molecules are well-known electron-rich compounds and they show efficient charge transport in photovoltaics applications.[28] Fused-thiophene derivatives lower the reorganization energy, a factor that has

[a] *B.-Y. Ke, M.-C. Kuo, Prof. T. J. Chow, Prof. S.-S. Sun*
Institute of Chemistry, Academia Sinica
No. 128, Sec. 2, Academia Road, Nankang, Taipei 115, Taiwan, (R.O.C.)
E-mail: sssun@chem.sinica.edu.tw
tjchow@chem.sinica.edu.tw

[b] *Prof. Y.-D. Lin,[+] H.-C. Chung, C.-C. Chou, H.-Y. Chen*
Department of Applied Chemistry, National Chiayi University
No. 300, Syuefu Road, Chiayi City 60004, Taiwan (R.O.C.)
E-mail: ydlin@mail.ncyu.edu.tw

[c] *Prof. K.-M. Lee[+]*
Department of Chemical and Materials Engineering, Chang Gung UniversityNo. 259, Wenhua 1st Road, Guishan Dist., Taoyuan City 33302, Taiwan (R.O.C.)
E-mail: kmlee@mail.cgu.edu.tw

[d] *Prof. K.-M. Lee[+]*
Division of Neonatology, Department of Pediatrics, Chang Gung Memorial Hospital, Linkou
5. Fu-Hsing St. Kuei Shan Hsiang, Taoyuan, Taiwan (R.O.C.)

[e] *Prof. K.-M. Lee[+]*
Center for Reliability Sciences and Technologies, Chang Gung University
No. 259, Wenhua 1st Road, Guishan Dist., Taoyuan 33302, Taiwan (R.O.C.)

[f] *K.-S. Chen, H.-C. Cheng, W.-J. Lin*
Department of Chemical and Material Engineering, National Central University
No. 300, Zhongda Road, Zhongli District, Taoyuan 32001, Taiwan (R.O.C.)

[g] *Prof. S. H. Chang*
Department of Physics, Chung Yuan Christian University
No. 200 Chung Pei Road, Zhongli District, Taoyuan 32023, Taiwan (R.O.C.)

[h] *Prof. C.-G. Wu, Prof. K.-L. Liau*
Department of Chemistry, National Central University
No. 300, Zhongda Road, Zhongli District, Taoyuan 32001, Taiwan (R.O.C.)

[i] *Prof. C.-G. Wu*
Research Center for New Generation Photovoltaics, National Central University
No. 300, Zhongda Road, Zhongli District, Taoyuan 32001, Taiwan (R.O.C.)

[j] *Prof. T. J. Chow*
Department of Chemistry, Tung Hai UniversityNo. 1727, Sec.4 Taiwan Boulevard, Xitun District, Taichung 40704 Taiwan (R.O.C)
E-mail: tjchow@chem.sinica.edu.tw

[+] *Y.-D. Lin and K.-M. Lee contributed equally to this work.*

Supporting information for this article is available on the WWW under https://doi.org/10.1002/ente.201800939

been shown to strongly affect the intermolecular hopping rate and hence the charge carries mobility in organic semiconductors.[29] Amongst these materials, cyclopenta[2,1-b;3,4-b′]dithiophene (CPDT) has been widely used as a building block in organic optoelectronics such as organic field-effect transistors (OFETs), organic photovoltaics (OPVs) and dye-sensitized solar cells (DSSCs) due to its excellent co-planarity and electron donating capability.[30–32] As an effective building block, the spiro-type derivatives based on 4-4′-spirobi[cyclopenta[2,1-b;3,4-b′]dithiophene] (spiro-CPDT) core connected by octyl-substituted bithiophenes as terminal moieties or *p*-methoxy-substituted triphenylamine groups have been investigated as potential HTMs for PSCs with PCEs of 10–13 %.[33,34] However, the synthesis of the spiro-CPDT core requires a complicated synthetic route.

In this study, we designed a series of two-dimensional CPDT-based HTMs connected by *p*-methoxytriphenylamine (**CT1** and **CT2**) and *p*-methoxydiphenylamine-substituted carbazole (**CT3** and **CT4**) with structures shown in Figure 1 as

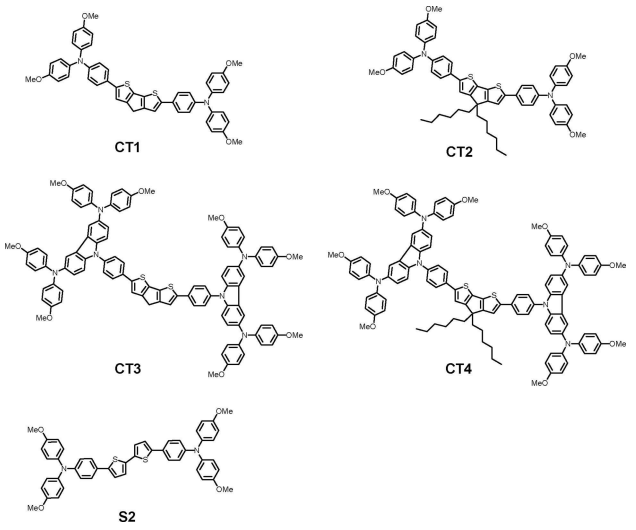

Figure 1. Chemical structures of CT series and S2.

the HTMs for PSCs. Their structures are simpler than spiro-CPDT based HTMs. In the structure of **CT2** and **CT4** HTMs, two aliphatic chains are attached to the bridging carbon atoms of CPDT in order to realize the influence of alkyl chains on the optoelectronic properties of the HTMs and the resulting PSCs. It is anticipated that the introduction of long alkyl chains on π-conjugated skeleton would significantly reduce the intermolecular interactions. In addition, to clarify the influence of the central core planarization on photovoltaic properties of solar cell devices, the 2,2′-dithiophene analogue **S2**[35] was prepared to serve as a reference material. The new semiconductors **CT** series and **S2** were tested as HTMs in perovskite solar cells using a device structure of FTO glass/TiO_2 compact layer/TiO_2 mesoporous/$CH_3NH_3PbI_3$/HTM/MoO_3/Ag. It was found that HTMs using the rigid and non-alkyl functionalized CPDT as the conjugated bridge showed better overall efficiencies (PCE = 17.71 % for **CT1** and PCE = 17.20 % for **CT3**) compared to their congeners with alkyl-functionalized CPDT HTMs (PCE = 15.59 % for **CT2** and PCE = 14.41 % for **CT4**) and non-fused bithiophene HTM **S2** (PCE = 8.55 %). By contrast, the spiro-OMeTAD HTM showed a 16.97 % of PCE under the similar condition. The origins of the significant improvement of PCEs based on **CT1** and **CT3** (without long alkyl chains) compared to **CT2** and **CT4** (alkyl-functionalized CPDT) and non-fused bithiophene **S2** were systematically investigated by morphological measurements and photoluminescence measurements. The uniformities of the HTMs **CT1** and **CT3** capping layer were significantly improved compared to those of **CT2**, **CT4** and **S2**. Photoluminescence studies indicated that **CT1** and **CT3** showed highly efficient hole transfer from the perovskite to HTMs. These results demonstrate that a two-dimensional and rigid π-framework plays an important role for HTMs to facilitate intramolecular π-conjugation and intermolecular π-π stacking, which provide both high charge carrier mobility and efficient intermolecular charge transfer to boost the device efficiency.[36] Moreover, the stability of CPDT-based devices exhibited excellent long-term stability over 1300 h. This work provides important information for the design and development of new type of simple and efficient HTMs for PSCs.

Results and Discussion

The synthetic scheme for the preparation of **CT** series is shown in Scheme 1 and the experimental details are provided

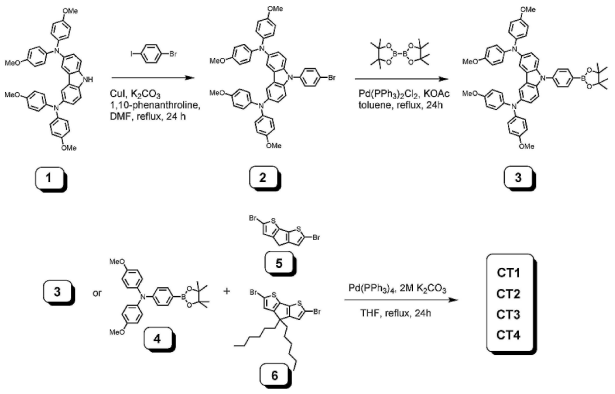

Scheme 1. Synthetic route for **CT** series.

in the ESI. The palladium-catalyzed C–N coupling of **1**[37] with 1-bromo-4-iodobenzene afforded compound **2**, which reacted with the commercially available bis(pinacol)borane in the presence of $PdCl_2(PPh_3)_2$ and KOAc in a refluxing toluene solution to provide the desired carbazole-based pinacoboronates **3**. The hole transporting material **CTs** were prepared from **3** or *N*-bis-(methoxyphenyl)-*N*-(4-(4,4,5,5-tetramethyl-1,3,2-dioxaborolan-2-yl)phenyl)amine (**4**) by Pd (0)-mediated Suzuki coupling reaction with 2,6-dibromo-4*H*-

cyclopenta-[2,1-b:3,4-b′]dithiophene (**5**) and 2,6-dibromo-4,4′-dihexyl-4*H*-cyclopenta[2,1-b:3,4-b′]dithiophene (**6**), respectively. All compounds were purified by column chromatography and characterized by $^{1}H/^{13}C$ NMR spectroscopy and high-resolution mass spectrometry.

The UV-vis absorption and fluorescence spectra of **CT** series and **S2** in chlorobenzene are depicted in Figure 2 and

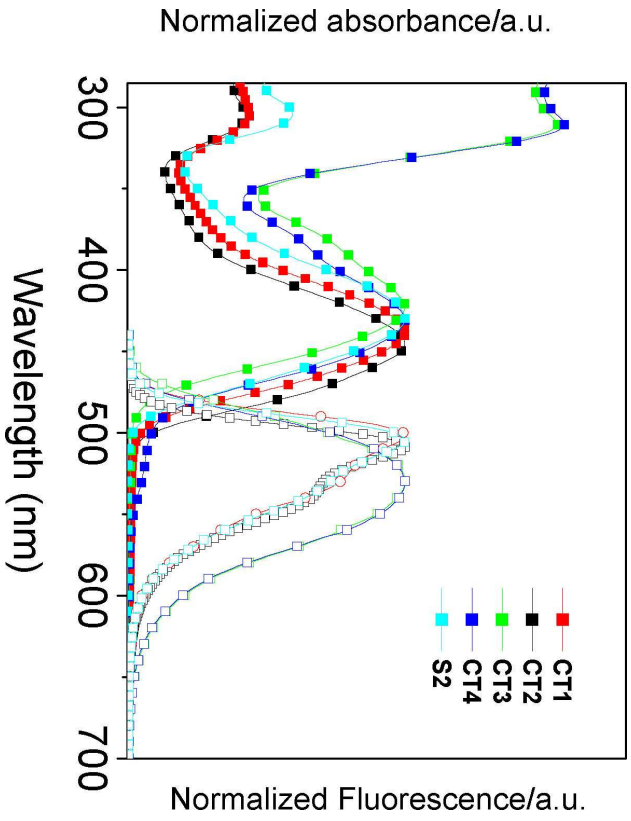

Figure 2. Absorption (■) and emission (□) spectra of the **CT** series and **S2** in chlorobenzene.

the photophysical data are summarized in Table 1. All the HTMs showed similar spectra with an absorption in the ultraviolet region (<350 nm) and an intense absorption band in the visible region. The maximum absorption bands of **CT1**, **CT2**, **CT3**, **CT4**, and **S2** were observed at 437, 445, 423, 431, and 430 nm, respectively. The maximal absorption bands in **CT1** and **CT2** are red shifted with respect to that in **S2**, indicative of a more delocalized electron distribution in the former HTMs. The fluorescence spectra of carbazole-based derivatives (**CT3** and **CT4**) showed the relatively large Stokes shifts between 4369–4808 cm^{-1} with respect to the triphenylamine-based derivatives (**CT1**, **CT2** and **S2** with Stokes shifts between 2787–3414 cm^{-1}), suggesting a significant structural change in excited state upon excitation. Compared to **CT1** and **CT3**, the additional two hexyl chains on CPDT core in **CT2** and **CT4** resulted in a slightly red shift of the absorption profiles and a decrease of the 0–0 band energy ($E_{0\text{-}0}$), estimated from the intersection of the corresponding normalized absorption and fluorescence spectra. The thermal analysis of all the HTMs was examined through thermogravimetric analysis (TGA) measurements. The TGA data indicate that all the HTMs are stable up to 400 °C (Figure S1).

The electrochemical properties of **CT** series and **S2** were examined by cyclic voltammetry (CV) (Figure S2) and differential pulse voltammetry (DPV) (Figure S3) in THF solutions ($1.0 \cdot 10^{-3}$ M). The redox parameters are collected in Table 1 and the HOMO-LUMO gaps are plotted in Figure 3. The first

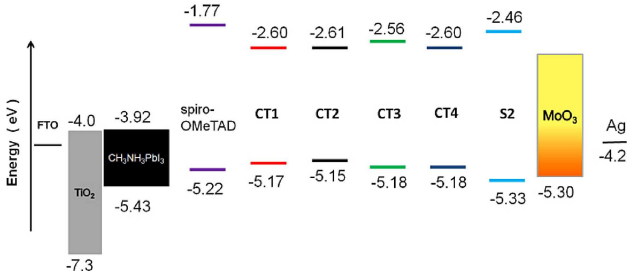

Figure 3. Energy level diagram of the hole-transporting materials used in perovskite solar cells.

oxidation potentials of **CT** series were found to be nearly the same. The HOMO values of **CT1**-**CT4** were determined to be −5.17, −5.15, −5.18 and −5.18 eV, respectively, which ensure sufficient driving force for hole extraction capability. **S2** possesses a higher oxidation potential than **CT** HTMs with the HOMO level of −5.33 eV. The lower HOMO level in **S2**

Table 1. Photophysical and electrochemical data of synthesized HTMs.

HTM	λ_{abs}[a] (nm) ($\varepsilon \cdot 10^{-4}/M^{-1}\,cm^{-1}$)	λ_f[a] (nm)	$\Delta\upsilon_{st}$[b] (cm^{-1})	E_{HOMO}[c] (eV)	$E_{0\text{-}0}$[d] (eV)	E_{LUMO}[e] (eV)	I_p[f] (eV)	E_{HOMO}[g] (eV)	E_{LUMO}[g] (eV)
CT1	437 (5.92)	502	2963	−5.17	2.57	−2.60	−5.00	−4.24	−1.31
CT2	445 (6.15)	508	2787	−5.15	2.54	−2.61	−4.97	−4.22	−1.33
CT3	423 (5.71)	531	4808	−5.18	2.62	−2.56	−5.10	−4.26	−1.76
CT4	431 (5.87)	531	4369	−5.18	2.58	−2.60	−5.07	−4.26	−1.76
S2	430 (6.91)	504	3414	−5.33	2.87	−2.46	−5.20	−4.41	−1.44
spiro-OMeTAD	389 (18.37)	428	2342	−5.22	3.03	−2.19	−5.14	−4.24	−2.23

[a] Maximum of the absorption and fluorescence band in chlorobenzene solution. [b] $\Delta\upsilon_{st} = \upsilon_{abs} - \upsilon_f$. [c] Determined from the differential pulse voltammetry. [d] The value of $\lambda_{0\text{-}0}$ was obtained from the intersection of normalized absorption and fluorescence spectra. [e] Energy of the LUMO of the compounds estimated by $E_{HOMO} - E_{0\text{-}0}$. [f] Ionization potential was measured by the photoemission yield spectroscopy in air method from films. [g] TDDFT/B3LYP/6-31G(d,p) level calculated values.

results in a slower hole transfer between the perovskite layers and **S2**, which contributes to a lower efficiency in PSCs in comparison with those of **CT** series (*vide infra*). The lower oxidation potentials for CPDT-based HTMs compared to that of **S2** can be ascribed to the more planar π-conjugated bridge. It is worth noting that the alkyl chains at the bridging carbon do not influence the HOMO levels of the molecules. Overall these results indicate that the appropriate HOMO levels could match with $CH_3NH_3PbI_3$ (−5.43 eV), revealing the favorable hole transfer from perovskite to the HTMs. For comparison, the HOMO value of spiro-OMeTAD was estimated to be −5.22 eV under the same experimental conditions.

To gain further understanding in energy level matching of the HTMs in PSCs, the photo-ionization energies (I_p) of **CT** series and **S2** thin film were measured by photoemission yield spectroscopy (PYS) (Figure S4). The measured I_p values for CPDT-based HTMs are similar to each other with −5.00, −4.97, −5.10, and −5.07 eV for **CT1**, **CT2**, **CT3**, and **CT4**, respectively. However, the I_p value of **S2** was lower (−5.20 eV) than all the above. The I_p values obtained from the PYS showed the same trend of the HOMO energy levels of the HTMs as that of the redox potentials measured by DPV.

To elucidate the molecular orbital properties and absorption spectra, density functional theory (DFT) and time-dependent density function theory (TDDFT) calculations were carried out based on B3LYP hybrid functional and 6–31G(d,p) basis set to obtain electronic density distributions of HOMO and LUMO levels and their energies (Figure S5, Table 1). The electron clouds of the HOMOs are distributed over the whole molecular backbone for **CT1**, **CT2** and **S2**, while the electron densities of the HOMOs of **CT3** and **CT4** are located at the carbazole moiety. The LUMOs of all HTMs are largely localized across the bithiophene moiety as well as adjacent phenyl rings. In addition, the calculations predict that for all HTMs there are two absorptions and the shape of the spectra and their trend agree well with the experimental results (Figure S6 and Table 1). Apparently, the optical, electrochemical and electronic properties of **CT1** and **CT3** are quite similar to those of **CT2** and **CT4** on the basis of their similar chemical structures.

The thin film crystallinity and morphologies of all the HTMs were investigated by powder X-ray diffraction (PXRD) and atomic force microscopy (AFM) to gain better understanding of the correlation between the morphology and device performance. As shown in PXRD (Figure S7), all CPDT-based HTMs present similar amorphous state in films, whereas **S2** displayed greater crystallinity than others, which may result in a reduction of charge carrier efficiency.[24,38] Moreover, three-dimensional AFM images and topography of glass/TiO_2/perovskite/HTM/MoO_3 film are shown in Figure 4. The root mean square (RMS) roughness is estimated to be 2.89, 7.40, 6.90, 14.27, and 15.21 nm for **CT1**, **CT2**, **CT3**, **CT4**, and **S2** cells, respectively. The results indicated that non-alkyl functionalized HTMs (**CT1** and **CT3**) showed more uniform thin film than the alkyl-functionalized congeners. The alkyl-

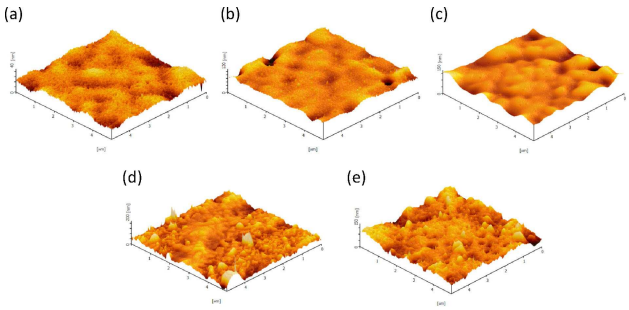

Figure 4. AFM three-dimensional surface plots of HTMs films based on (a) **CT1**, (b) **CT2**, (c) **CT3**, (d) **CT4**, and (e) **S2**.

functionalized (**CT2** and **CT4**) and non-fused HTMs (**S2**) presented considerable surface roughness and thickness non-uniformity, which result in low-resistance shunting paths and, thus, affect the charge transport properties in PSCs and device stability.[39] The films of the **CT1** and **CT3** exhibit more ordered structures, which is beneficial to charge transportation, leading to an increase in J_{sc} as well as device efficiency.

Charge transport properties of the HTMs were further studied by measuring space-charge-limited current (SCLC) in the *J-V* characteristics obtained under a dark condition (Figure S8). The hole mobility of **CT1**, **CT2**, **CT3**, **CT4**, and **S2** are $3.21\cdot10^{-4}$, $2.33\cdot10^{-4}$, $3.18\cdot10^{-4}$, $5.75\cdot10^{-5}$, and $6.76\cdot10^{-5}$ $cm^2V^{-1}s^{-1}$, respectively. The value of mobility obtained here ($3.58\cdot10^{-4}$) for spiro-OMeTAD is similar to the data reported in the literature and our previous work.[24,40] The mobility depends on the molecular structure and intermolecular packing, and hence influence charge transport. The hole mobility values of **CT1** and **CT3** are higher than those of **CT2** and **CT4**, which suggest that the former HTMs based devices should yield higher fill factors. It can be seen that incorporation of the alkyl chains to CPDT (**CT2** and **CT4**) may impede the π–π stacking of aromatic cores and lead to the reduction of hole mobility. In contrast, the improved hole mobility for **CT1** and **CT3** with respect to the analogues **CT2** and **CT4** is likely due to decreased π–π stacking distances. Furthermore, the hole mobilities of fused-ring HTMs (**CT1** and **CT3**) exhibit about one order of magnitude higher than that of non-fused bithiophene (**S2**). The much lower hole mobility values of **S2** may be attributed to the irregular molecular packing of nonplanar bithiophene core.

PSCs were fabricated with **CT** series and **S2** as the HTMs to assess the effect of π-bridges within the structure of HTMs on the device performance. The HTM layers were deposited onto the perovskite films containing tri(bis(trifluoromethylsulfonyl)imide) (Li-TFSI) and *tert*-butylpyridine (*t*BP) as the additives. The device configuration is FTO/blocking layer-TiO_2/mp-TiO_2/perovskite/HTM/MoO_3/Ag. The MoO_3 used here not only formed a high work function contact buffer for efficient hole injection/extraction but also protected the organic films from damage caused by Ag deposition.[41–43] A representative cross-sectional image is shown in Figure 5 analyzed by scanning electron microscopy (SEM), which exhibited a well-defined layer-by-layer structure with clear

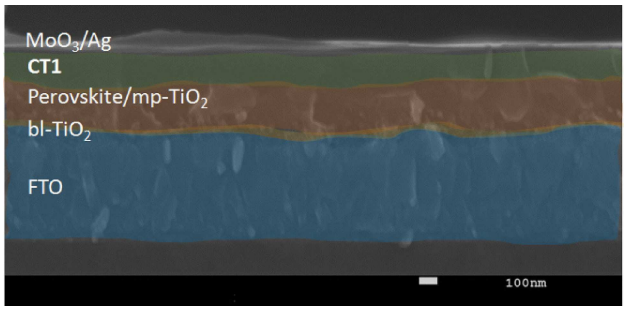

Figure 5. Cross-sectional SEM image of the device of FTO/bl-TiO_2/mp-TiO_2/perovskite/**CT1**/MoO_3/Ag.

interfaces. The thickness of mesoporous TiO_2 layer incorporated with perovskite, HTM layer, MoO_3 layer, and Ag electrode were approximately 300, 250, 15, and 100 nm, respectively. The optimized photovoltaic parameters are listed in Table 2 and the corresponding current-voltage (*J-V*) characteristics of PSCs measured under 100 mW cm^{-2} AM 1.5G illumination for reverse scan condition are shown in Figure 6.

Table 2. Summary of photovoltaic characteristics extracted from *J-V* curves of perovskite solar cells.[a]

HTM	J_{sc}/mA cm^{-2}	V_{oc}/V	FF (%)	PCE(%)
CT1	22.45 ± 0.14	1.03 ± 0.02	76.6 ± 0.5	17.71 ± 0.07
CT2	21.02 ± 0.22	1.03 ± 0.04	72.0 ± 0.5	15.59 ± 0.08
CT3	22.22 ± 0.15	1.02 ± 0.02	75.9 ± 0.4	17.20 ± 0.07
CT4	21.05 ± 0.17	1.01 ± 0.03	67.8 ± 0.7	14.41 ± 0.07
S2	20.71 ± 0.28	0.94 ± 0.04	43.9 ± 0.8	8.55 ± 0.08
spiro-OMeTAD	22.11 ± 0.18	1.03 ± 0.01	74.0 ± 0.5	16.97 ± 0.05

[a] Performances of devices were measured using a 0.16 cm^2 working area and the data was calculated based on 8 cells.

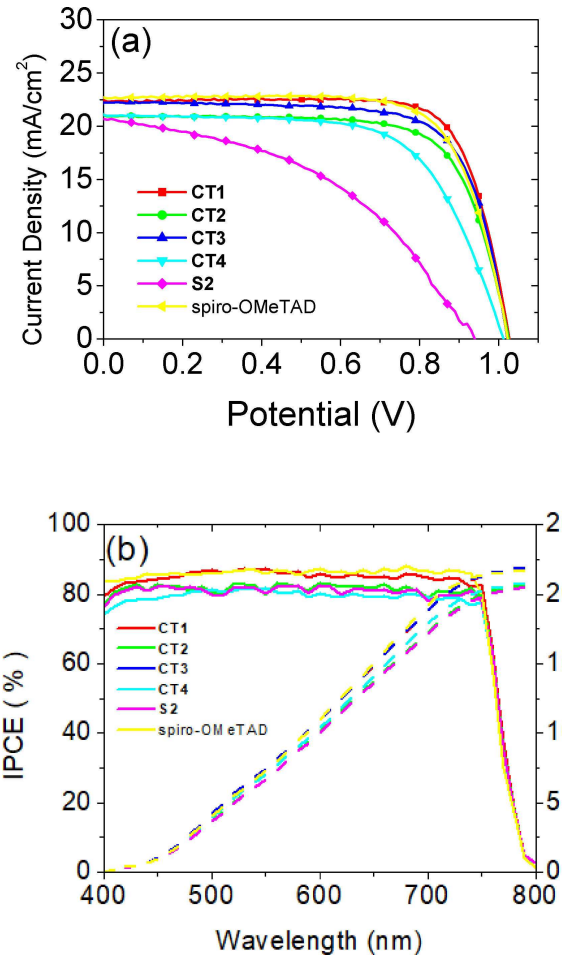

Figure 6. (a) Plots of *J-V* curves for the perovskite solar cells using **CT** series, **S2**, and spiro-OMeTAD. (b) The IPCE spectra of solar cells based on **CT** series, **S2**, and spiro-OMeTAD. Dashed lines indicate the calculated J_{sc} from integrated IPCE values.

The PCEs of the devices with **CT** series and **S2** were measured to be 17.71, 15.59, 17.20, 14.41, and 8.55 % for **CT1**, **CT2**, **CT3**, **CT4**, and **S2**, respectively (Table 2). The PCE of the best performing device with **CT1** as the HTM is 17.71 % with a V_{oc} of 1.03 V, a J_{sc} of 22.45 mA cm^{-2} and a FF of 76.6 %. In addition, a reference cell with spiro-OMeTAD as the HTM was also fabricated under the same conditions, obtaining a PCE of 16.97 %, with a V_{oc} of 1.03 V, a J_{sc} of 22.11 mA cm^{-2} and a fill factor of 0.74 under reverse scan conditions. We noticed that the photovoltaic devices exhibited hysteresis in the *J-V* curves (Figure S9, Table S1) where the PSCs are well known to show such behavior due to the poor electron conductivity of TiO_2.[44] A comparison between the two analogous pairs of **CT1**/**CT2** and **CT3**/**CT4** is noteworthy. It is obvious that the CPDT-based HTMs without alkyl chains (**CT1** and **CT3**) show higher efficiencies than those of the alkyl-functionalized **CT2** and **CT4** counterparts mainly due to the increased J_{sc} and FF values. These results could be attributed to the more efficient charge transfer from perovskite layer to the HTMs associated with the relatively higher hole mobility and better HTM surface uniformity (Figure 4) in devices with **CT1** and **CT3**. In contrast, the device based on **S2** produced a much lower efficiency of 8.55 % mainly caused by the low V_{oc} and FF, which might be attributed to three possible factors: (a) a much lower HOMO level of **S2**, which decreases the efficiency of hole transfer from the perovskite to HTM layer; (b) a low hole mobility, which might lead to serious serial resistance; (c) a poor surface uniformity, which increases interfacial charge recombination to reduce charge collection efficiency. These together lead to a lower PCE in nonbridged **S2**-based PSC compared to ring-bridged **CT** series. We noticed that all the CPDT-based HTMs are quite similar in terms of V_{oc}, which may be rationalized by the similar HOMO levels of the HTMs. Apparently, the photovoltaic performance is quite sensitive to structural change. We demonstrate that two-dimensional CPDT-based HTMs without alkyl chains (**CT1** and **CT3**) show a better performance in PSC photovoltaic device than many other HTMs reported in literature (Table S3), which can be attributed to the improved intermolecular packing structure on the basis of their coplanar central skeleton, thus benefiting charge transport. By holding a bias near the

maximum power output point (0.82 V), the photocurrent density and PCE as a function of time at the maximum power point were estimated. As shown in Figure 7, the photocurrent

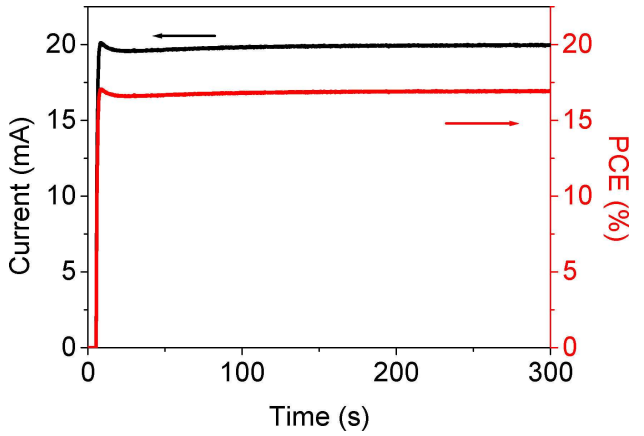

Figure 7. Steady-state photocurrent measurement of the **CT1** cell at a bias voltage (0.82 V) near the maximum power point and stabilized power output.

and PCE remained stable across a 300 s scan. A stabilized efficiency over 17 % was demonstrated, which matches the *J-V* curve reasonably well. This indicates that the test conditions provide an accurate representation of the cells' photovoltaic performance. The incident photon to current conversion efficiency (IPCE) spectra of the optimized perovskite devices based on six HTMs are shown in Figure 6b. The photocurrent densities of **CT1**, **CT2**, **CT3**, **CT4**, **S2** and spiro-OMeTAD are 20.90, 20.04, 20.12, 19.53, 19.86, and 20.98 mA cm^{-2}, respectively, from the IPCE spectra, which are in good agreement with the J_{sc} values measured from the *J-V* curves. The **CT1** and **CT3** devices exhibit higher IPCE values in the range of 400–750 nm compared with the **CT2** and **CT4** counterparts devices. To confirm the reproducibility, 40 independent devices were fabricated and tested for PSCs. The efficiency histogram of the cell performance characteristics are shown in Figures 8 and S10. The average V_{oc}, J_{sc}, FF, and PCEs are 1.01 V, 21.3 mA cm^{-2}, 0.71 and 15.5 %, respectively, indicating the high quality and performance stability of the perovskite solar cells. Furthermore, we also fabricated perovskite devices using **CT** series and **S2** HTMs without MoO_3 layer (Figure S11 and Table S2). However, all the devices exhibited lower photovoltaic performance compared with the ones with MoO_3, indicating that MoO_3 layer is necessary to reach a high efficiency for **CT** series and **S2**. It is worth noting that all the devices with MoO_3 mainly show a higher J_{sc} and FF.

To further investigate the hole transfer process at the interface, we measured the steady-state photoluminescence (PL) spectra of FTO/perovskite and FTO/perovskite/HTM films, which are presented in Figure 9. The quenching of steady-state PL serves as an indicator of efficient charge extraction at the perovskite/HTM interface. The perovskite shows a strong PL band near 760 nm, whereas a dramatic reduction of the emission with respect to the pristine

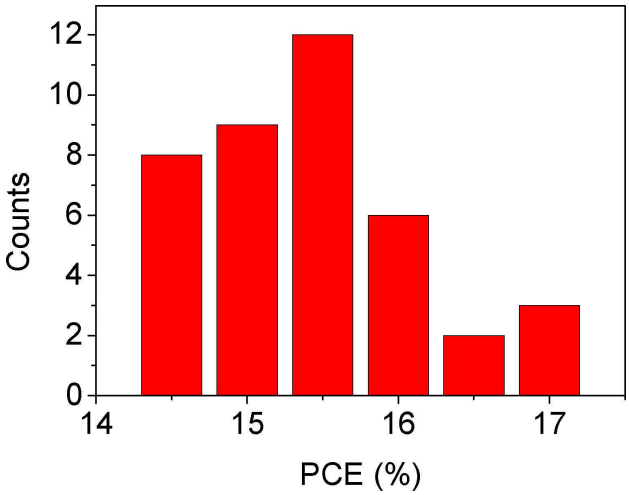

Figure 8. Histogram of PCE measured using backward scans for 40 devices based on **CT1** HTM.

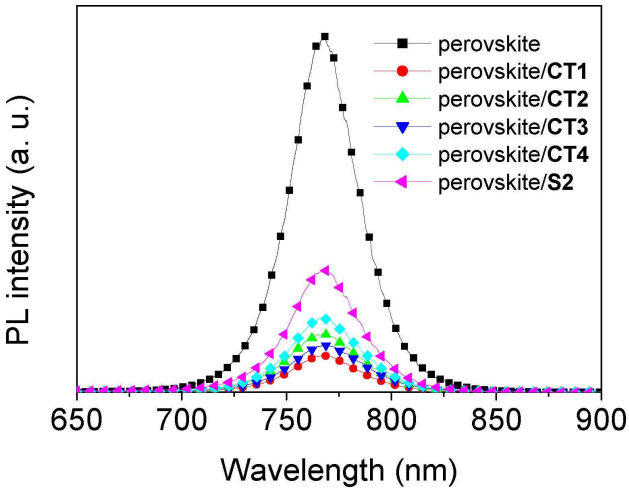

Figure 9. Steady-state photoluminescence spectra of perovskite film with and without HTMs.

perovskite can be observed upon coating the HTM onto the perovskite films, indicative of significant hole extraction from perovskite into HTM. It is evident that **CT1** and **CT3** showed more efficient PL quenching (ca. 88 % for **CT1** and 86 % for **CT3**) relative to **CT2** (ca. 82 %) and **CT4** (ca. 78 %), which means that the former HTMs extracted holes more efficiently. It may be a reason of the higher J_{sc} of **CT1** and **CT3**-based PSCs compared to **CT2** and **CT4**-based devices. This could be attributed to the alkyl chains on CPDT core that hinder π-π stacking and result in less efficient hole transport.[45] In contrast, for HTM **S2**, the PL intensity was reduced to roughly 65 % of the pristine films, indicating a less efficient hole transfer between the perovskite and **S2**. Consequently, the result from steady-state PL confirms that the coplanar skeleton on CPDT-based HTMs plays an important role to benefit hole transport, and thus exhibits a higher efficiency in PSCs.

Stability is still a key issue for practical application of PSCs. The long-term stability of **CT1**, **CT2**, **S2**, and spiro-OMeTAD perovskite solar cells without encapsulation were examined and the results are shown in Figure 10. All cells

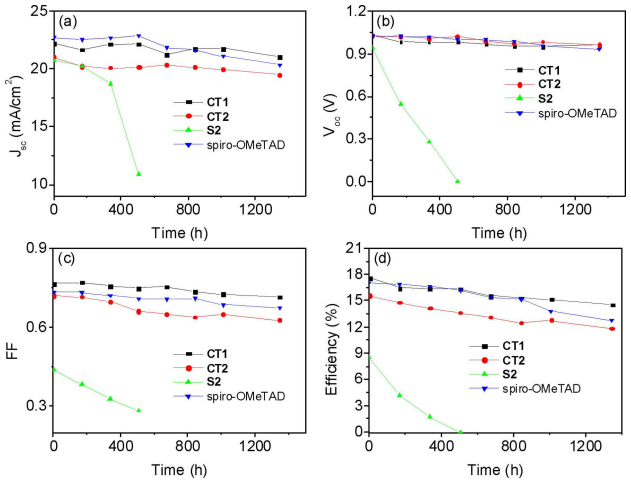

Figure 10. Stability test for devices based on **CT1**, **CT2**, **S2**, and spiro-OMeTAD in a low humidity atmosphere (2 RH %).

were unsealed and kept in dark in a low humidity atmosphere (<2 RH %). The PCEs of the device with **CT1**, **CT2**, and spiro-OMeTAD as the HTMs exhibited that there is ca. 14 %, 25 % and 25 % efficiency drops relative to the initial PCE over 1300 h. In contrast, the efficiency of **S2** device showed rapid degradation and vanished after 500 h. In order to further study the effect of the HTMs on the cells stability, we investigated the surface morphologies of the **CT1**, **CT2**, **S2**, and spiro-OMeTAD layers on the surface of the perovskite material using SEM imaging (Figure S12a). It was found that **CT1**, **CT2**, and spiro-OMeTAD based perovskite film exhibits a compact and homogeneous HTM capping layer without any pinholes. However, the **S2** layer contains some rectangle-shaped islands morphology with inhomogeneous coverage, indicating that **S2** tends to form aggregation or crystallization, which is in good agreement with the PXRD power pattern (Figure S7). After 5 days, **CT1**, **CT2**, and spiro-OMeTAD based perovskite film did not show apparent morphology change (Figure S12b), which effectively prevents the moisture penetration through HTM layer to the perovskite layer.[39,46] In contrast, the **S2** layer presented a larger amount of rectangle-shaped crystals in the film, leading to incomplete surface coverage, thus causing the degradation of the perovskite materials. These results demonstrated that CPDT-based HTMs significantly enhance the stability of perovskite solar cells, which may also be ascribed to the uniform and smooth HTMs film.

Conclusions

In conclusion, we have designed a series of small molecule-based HTMs with a CPDT-core and utilized these HTMs to produce highly efficient perovskite solar cells with excellent long-term stability. The systematic studies on **CT** series and **S2** provided important insights into the correlation between the chemical structures of HTMs and the photovoltaic performance of the PSCs. The solar cell prepared with ring-bridged **CT** series exhibited a considerably higher performance than that prepared with the non-bridged **S2** due to an appropriate HOMO energy level, more uniform capping layer on perovskite layer, effective hole injection ability from the perovskite layer into the HOMO of HTMs, and higher hole mobility. These results demonstrated that rigid π-skeleton on CPDT-based HTMs should be particularly beneficial. In addition, our results indicate that CPDT-based HTMs without two alkyl groups enable better photovoltaic performance than those with alkyl-functionalized CPDT HTMs, which is attributed to more efficient transport of hole carriers and to more uniformly cap the perovskite layer. Moreover, steady-state photoluminescence (PL) indicated that **CT1** and **CT3** are more effective in quenching the excited perovskite than those of the **CT2** and **CT4**, revealing an improved hole extraction for the former HTMs. The PSCs based on **CT1** as the HTM shows an excellent PCE of 17.71 %, which is on par with that obtained employing the state-of-the-art spiro-OMeTAD (16.97 %). Thus we demonstrate that a subtle change of the central π-bridge unit can lead to a significant improvement of device performance. Moreover, the devices based on **CT1** obtained a higher stability after 1300 h than the device based on spiro-OMeTAD without encapsulation. The present results indicate that these new two-dimensional CPDT-based materials are promising HTMs for fabricating efficient and stable perovskite photovoltaic devices.

Experimental Section

General information

All solvents and chemicals were purchased from Aldrich, ACROS, Alfa, Merck, Lancaster, TCI, Showa, and Sigma-Aldrich, separately. The thin-layer chromatography (TLC) was conducted with Merck KGaA precoated TLC Silica gel 60F254 aluminum sheets. Flash column chromatography was performed on glass columns packed with silica gel using Silicycle UltraPure SilicaFlash P60, 40–63 mm (230–400 mesh). Unless otherwise specified, all reactions and manipulations were carried out under a nitrogen atmosphere and the purity of all commercial materials and solvents were more than 98 %. Solvents of reagent grade were used for syntheses and those of spectroscopy grade for spectral measurements. Solvents were dried by standard procedures. ^{1}H and ^{13}C NMR spectra were recorded on a Bruker 400 and 600 MHz spectrometer. Fast atom bombardment (FAB) mass spectra were recorded on a Jeol JMS 700 double-focusing spectrometer. UV spectra were measured on a Jasco V-530 double beam spectrophotometer. Fluorescence spectra were recorded on a Hitachi F-4500 fluorescence spectrophotometer. CV experiments were performed with a CHI-621 A electro-

chemical analyzer. All measurements were carried out at room temperature with a conventional three electrode configuration that consisted of a platinum working electrode, an auxiliary electrode, and a nonaqueous $Ag/AgNO_3$ reference electrode. The SEM images were obtained by using a field-emission scanning electron microscope (JEOL-7401). The AFM images were obtained by using a Nano-Scope NS3 A system (Digital Instrument) to observe the surface morphologies and thicknesses of various thin films

Synthesis of 2

Compound **1** (1.9 g, 3.1 mmol), 1-bromo-4-iodobenzene (1.72 g, 6.1 mmol), 1,10-phenanthroline (0.11 g, 0.2 eq), CuI (0.058 g, 0.1 eq), and K_2CO_3 (0.89 g, 2.1 eq) in 31 mL of anhydrous DMF under nitrogen was heated at 130 °C for 16 h. After cooling, the reaction solution was extracted with CH_2Cl_2. The combined organic layer was dried over $MgSO_4$ and evaporated under reduced pressure. Further purification was performed by column chromatography, using a mixed solvent CH_2Cl_2/hexane (1/1) as the eluent to provide yellow solid in 83 % yield. mp 121–122 °C; ^{1}H NMR (400 MHz, DMSO-d_6, δ): 7.83 (d, J = 8.0 Hz, 2 H), 7.71 (d, J = 4.0 Hz, 2 H), 7.59 (d, J = 8.0 Hz, 2 H), 7.31 (d, J = 8.0 Hz, 2 H), 7.08 (m, 2 H), 6.88 (m, 16 H), 3.69 (s, 12 H) ppm; ^{13}C NMR (100 MHz, DMSO-d_6, δ): 154.9, 142.3, 142.4, 142.0, 137.3, 136.8, 133.6, 129.2, 125.0, 124.5, 120.5, 116.9, 115.2, 111.2, 55.7 ppm; HRMS (FAB) m/z [M$^+$] calcd for $C_{46}H_{38}O_4N_3Br$: 775.2046; found: 775.2017.

Synthesis of 3

Compound **2** (2.0 g, 2.6 mmol), bis(pinacol)diboron (0.79 g, 3.12 mmol), KOAc (0.77 g, 7.8 mmol), and $Pd(PPh_3)_2Cl_2$ (0.234 g, 5 mol%) in 26 mL of anhydrous toluene under nitrogen was heated at 120 °C for 18 h. The solution was cooled and then 30 mL of CH_2Cl_2 was added. The insoluble residue was filtered off and the filtrate was concentrated *in vacuo* to afford the crude product. Further purification was performed by column chromatography, using a mixed solvent CH_2Cl_2/hexane (2/1) as the eluent to provide yellow solids in 76 % yield. mp 132–133 °C; ^{1}H NMR (600 MHz, DMSO-d_6, δ): 7.93 (d, J = 7.8 Hz, 2 H), 7.70 (s, 2 H), 7.62 (d, J = 7.8 Hz, 2 H), 7.34 (d, J = 9.0 Hz, 2 H), 7.07 (d, J = 9.0 Hz, 2 H), 6.87 (d, J = 8.4 Hz, 8 H), 6.81 (d, J = 8.4 Hz, 8 H), 3.69 (s, 12 H), 1.33 (s, 12 H) ppm; ^{13}C NMR (150 MHz, DMSO-d_6, δ): 154.8, 142.3, 142.0, 140.2, 137.1, 136.7, 135.0, 126.1, 124.9, 124.5, 124.1, 116.8, 115.2, 111.3, 84.4, 55.7, 25.2 ppm; HRMS (FAB) m/z [M$^+$] calcd for $C_{52}H_{50}O_6N_3B$: 823.3793; found: 823.3797.

Synthesis of CT1

A heterogeneous mixture of 2 M K_2CO_3 (8 mL), THF (10 mL), **4** (1.32 g, 3.05 mmol), **5** (0.5 g, 1.49 mmol), and $Pd(PPh_3)_4$ (0.069 g, 4 mol %) under argon was heated at 80 °C for 18 h. The mixture was extracted with CH_2Cl_2. The organic layer was dried over anhydrous $MgSO_4$. Evaporation of the solvent gave a crude product, which was purified by silica gel column chromatography eluted with CH_2Cl_2/hexane (1/1) to afford the desired product as a yellow solid in 72 % yield. mp 128–129 °C; ^{1}H NMR (400 MHz, DMSO-d_6, δ): 7.46 (d, J = 8.4 Hz, 4 H), 7.43 (s, 2 H), 7.04 (d, J = 8.2 Hz, 8 H), 6.93 (d, J = 8.2 Hz, 8 H), 6.78 (d, J = 8.4 Hz, 4 H), 3.75 (s, 12 H), 3.65 (s, 2 H) ppm; ^{13}C NMR (100 MHz, DMSO-d_6, δ): 156.4, 150.8, 148.1, 144.1, 140.3, 136.22, 127.2, 126.2, 120.0, 118.8, 117.1 115.5, 55.7, 33.8 ppm; HRMS (FAB) m/z [M$^+$] calcd for $C_{49}H_{40}O_4N_2S_2$: 784.2429; found: 784.2435.

Synthesis of CT2

A heterogeneous mixture of 2 M K_2CO_3 (5 mL), THF (7 mL), **4** (0.94 g, 2.2 mmol), **6** (0.5 g, 1.00 mmol), and $Pd(PPh_3)_4$ (0.046 g, 4 mol %) under argon was heated at 80 °C for 18 h. The mixture was extracted with CH_2Cl_2. The organic layer was dried over anhydrous $MgSO_4$. Evaporation of the solvent gave a crude product, which was purified by silica gel column chromatography eluted with CH_2Cl_2/hexane (1/1) to afford the desired product as a yellow solid in 78 % yield. mp 108–109 °C; ^{1}H NMR (600 MHz, DMSO-d_6, δ): 7.47 (d, J = 8.4 Hz, 4 H), 7.35 (s, 2 H), 7.03 (d, J = 9.0 Hz, 8 H), 6.93 (d, J = 9.0 Hz, 8 H), 6.79 (d, J = 8.4 Hz, 4 H), 3.75 (s, 12 H), 1.84–1.87 (m, 4 H), 1.11–1.25 (m, 12 H), 0.90–0.92 (m, 4 H), 0.77 (t, J = 6.4 Hz, 6 H) ppm; ^{13}C NMR (150 MHz, DMSO-d_6, δ): 158.9, 156.3, 148.0, 144.3, 140.4, 134.2, 127.0, 126.1, 120.3, 118.3, 117.3, 115.5, 55.7, 54.1, 37.6, 31.5, 29.5, 24.5, 22.5, 14.3 ppm; HRMS (FAB) m/z [M$^+$] calcd for $C_{61}H_{64}O_4N_2S_2$: 952.4307; found: 952.4325.

Synthesis of CT3

A heterogeneous mixture of 2 M K_2CO_3 (3 mL), THF (4 mL), **3** (0.70 g, 0.85 mmol), **5** (0.14 g, 0.4 mmol), and $Pd(PPh_3)_4$ (0.018 g, 4 mol%) under argon was heated at 80 °C for 18 h. The mixture was extracted with CH_2Cl_2. The organic layer was dried over anhydrous $MgSO_4$. Evaporation of the solvent gave a crude product, which was purified by silica gel column chromatography eluted with CH_2Cl_2/hexane (2/1) to afford the desired product as a yellow solid in 92 % yield. mp 197–198 °C; ^{1}H NMR (600 MHz, DMSO-d_6, δ): 7.89 (d, J = 8.4 Hz, 4 H), 7.73 (s, 2 H), 7.65 (s, 4 H), 7.57 (d, J = 8.4 Hz, 4 H), 7.26 (d, J = 8.4 Hz, 4 H), 7.05 (d, J = 8.4 Hz, 4 H), 6.84 (d, J = 8.2 Hz, 16 H), 6.77 (d, J = 8.2 Hz, 16 H), 3.74 (s, 2 H), 3.67 (s, 24 H) ppm; ^{13}C NMR (150 MHz, DMSO-d_6, δ): 154.8, 151.6, 143.3, 142.4, 141.8, 138.0, 137.5, 136.1, 133.9, 127.6, 126.7, 125.1, 124.4, 123.9, 121.0, 117.1, 115.1, 111.3, 55.6, 33.4 ppm; HRMS (FAB) m/z [M+H]$^+$ calcd for $C_{101}H_{81}O_8N_6S_2$: 1569.5557; found: 1569.5552.

Synthesis of CT4

A heterogeneous mixture of 2 M K_2CO_3 (2 mL), THF (3 mL), **3** (0.63 g, 0.76 mmol), **6** (0.18 g, 0.36 mmol), and $Pd(PPh_3)_4$ (0.017 g, 4 mol%) under argon was heated at 80 °C for 18 h. The mixture was extracted with CH_2Cl_2. The organic layer was dried over anhydrous $MgSO_4$. Evaporation of the solvent gave a crude product, which was purified by silica gel column chromatography eluted with CH_2Cl_2/hexane (2/1) to afford the desired product as an orange solid in 88 % yield. mp 180–181 °C; ^{1}H NMR (400 MHz, DMSO-d_6, δ): 7.91 (d, J = 8.4 Hz, 4 H), 7.73 (s, 2 H), 7.70 (s, 4 H), 7.59 (d, J = 8.4 Hz, 4 H), 7.28 (d, J = 8.8 Hz, 4 H), 7.07 (d, J = 8.8 Hz, 4 H), 6.87 (d, J = 8.2 Hz, 16 H), 6.80 (d, J = 8.2 Hz, 16 H), 3.68 (s, 24 H), 1.92–1.95 (m, 4 H), 1.10–1.25 (m, 12 H), 0.90–0.92 (m, 4 H), 0.77 (t, J = 6.4 Hz, 6 H) ppm; ^{13}C NMR (100 MHz, DMSO-d_6, δ): 159.4, 154.6, 143.5, 142.4, 141.7, 137.5, 136.3, 135.7, 134.1, 127.4, 126.4, 125.3, 124.2, 123.8, 119.4, 117.3, 115.1, 111.1, 55.5, 54.1, 37.5, 31.4, 29.5, 24.4, 22.5, 14.2 ppm; HRMS (FAB) m/z [M+H]$^+$ calcd for $C_{113}H_{105}O_8N_6S_2$: 1737.7435; found: 1737.7395.

Device fabrication

A TiO_2 compact layer (~30 nm in thickness) was deposited by spin-coating a titanium isopropyl solution onto a F:SnO_2 (FTO) substrate. A 150 nm-thick mesoporous TiO_2 film (particle size: ~20 nm, crystalline phase: anatase) was spin-coating onto the

compact-TiO_2/FTO substrate using home-made pastes and heated to 500 °C for 30 minutes. After sintering the TiO_2 layer, the electrode was cooled to room temperature and immersed in 0.04 M aqueous $TiCl_4$ at 70 °C for 30 min. The film was then rinsed by deionized water and then annealed at 500 °C for 30 min again. After cooling to room temperature the substrate was transferred to a nitrogen filled glove box. A solution consisting of PbI_2 (1.25 M) and methylammoniumiodide (1.25 M) in GBL and DMSO (7/3, v/v) was coated by two-step spin-coating process at 1000 and 5000 rpm for 10 and 20 s, respectively onto the substrate. During the second spin-coating step, the substrate was treated with 50 µL toluene drop-casting. The substrate was dried on a hot plate at 100 °C for 10 min. A solution of HTMs (**CT1**, **CT2**, **CT3**, **CT4**, **S2** and spiro-OMeTAD) was mixed with 17.5 µL of a solution of lithium bis-trifluoromethanesulfonimide (Li-TSFI, 520 mg) in acetonitrile (1 mL) and 28.5 µL 4-*tert*-butylpyridine and spin-coated on substrate at 2000 rpm for 30 s. The MoO_3 was deposited by thermal evaporation (~15 nm). Finally, the Ag counter electrode was deposited by thermal evaporation (~100 nm). The active area of this electrode was fixed at 0.16 cm^2. *J-V* curves were recorded with a Keithley 2400 source meter under simulated AM 1.5G sunlight, calibrated to 100 mW/cm^2. The reported device characteristics were estimated from the measured *J-V* curves.

Acknowledgements

We are grateful to Academia Sinica (AS-KPQ-106-DDPP) for support of this research. Y.-D. Lin thanks the support from Ministry of Science and Technology, Taiwan (Grant No MOST 107-2113-M-415-006-). K.-M. Lee thanks the support from Ministry of Science and Technology, Taiwan (MOST 106-2218-E-182-005-MY2) and Chang Gung Memorial Hospital, Linkou, Taiwan (CMRPD2G0301).

Conflict of interest

The authors declare no conflict of interest.

Keywords: perovskite solar cell · hole transporting materials · cyclopenta[2,1-b;3,4-b′]dithiophene · long-term stability

[1] A. Kojima, K. Teshima, Y. Shirai, T. Miyasaka, *J. Am. Chem. Soc.* **2009**, *131*, 6050.
[2] S. D. Stranks, G. E. Eperon, G. Grancini, C. Menelaou, M. J. P. Alcocer, T. Leijtens, L. M. Herz, A. Petrozza, H. J. Snaith, *Science* **2013**, *342*, 341.
[3] G. Hodes, *Science* **2013**, *342*, 317.
[4] M. Grätzel, *Nat. Mater.* **2014**, *13*, 838.
[5] M. Saliba, T. Matsui, K. Domanski, J.-Y. Seo, A. Ummadisingu, S. M. Zakeeruddin, J.-P. Correa-Baena, W. R. Tress, A. Abate, A. Hagfeldt, M. Grätzel, *Science* **2016**, *354*, 206.
[6] M. Saliba, T. Matsui, J.-Y. Seo, K. Domanski, J. P. Correa-Baena, M. K. Nazeeruddin, S. M. Zakeeruddin, W. Tress, A. Abate, A. Hagfeldt, M. Grätzel, *Energy Environ. Sci.* **2016**, *9,* 1989.
[7] K. Domanski, J.-P. Correa-Baena, N. Mine, M. K. Nazeeruddin, A. Abate, M. Saliba, W. Tress, A. Hagfeldt, M. Grätzel, *ACS Nano* **2016**, *10*, 6306.
[8] W. S. Yang, B.-W. Park, E. H. Jung, N. J. Jeon, Y. C. Kim, D. U. Lee, S. S. Shin, J. Seo, E. K. Kim, J. H. Noh, S. I. Seok, *Science* **2017**, *356*, 1376.
[9] P. Ganesan, K. Fu, P. Gao, I. Raabe, K. Schenk, R. Scopelliti, J. Luo, L. H. Wong, M. Grätzel, M. K. Nazeeruddin, *Energy Environ. Sci.* **2015**, *8*, 1986.
[10] P. Qin, S. Tanaka, S. Ito, N. Tetreault, K. Manabe, H. Nishino, M. K. Nazeeruddin, M. Grätzel, *Nat. Commun.* **2014**, *5*, 3834.
[11] N. J. Jeon, J. H. Noh, W. S. Yang, Y. C. Kim, S. Ryu, J. Seo, S. I. Seok, *Nature* **2015**, *517*, 476.
[12] P. Qin, S. Tanaka, S. Ito, N. Tetreault, K. Manabe, H. Nishino, M. K. Nazeeruddin, M. Grätzel, *Nat. Commun.* **2014**, *5*, 3834.
[13] W. S. Yang, J. H. Noh, N. J. Jeon, Y. C. Kim, S. Ryu, J. Seo, S. I. Seok, *Science* **2015**, *348*, 1234.
[14] B. Xu, J. Zhang, Y. Hua P. Liu, L. Wang, C. Ruan Y. Li, G. Boschloo, E. M. J. Johansson, L. Kloo A. Hagfldt, A. K.-Y. Jen, L. Sun, *Chem* **2017**, *2*, 676.
[15] F. Zhang Z. Wang H. Zhu N. Pellet, J. Luo C. Yi, X. Liu, H. Liu S. Wang, X. Li, Y. Xiao S. M. Zakeeruddin, D. Bi, M. Grätzel *Nano Energy* **2017**, *41*, 469.
[16] N. J. Jeon, H. G. Lee, Y. C. Kim, J. Seo, J. H. Noh, J. Lee, S. I. Seok, *J. Am. Chem. Soc.* **2014**, *136*, 7837.
[17] B. Xu, D. Bi, Y. Hua, P. Liu, M. Cheng, M. Grätzel, L. Kloo, A. Hagfeldt,, L. Sun, *Energy Environ. Sci.* **2016**, *9*, 873.
[18] C. Huang, W. Fu, C. Z. Li, Z. Zhang, W. Qiu, M. Shi, P. Heremans, A. K. Jen, H. Chen, *J. Am. Chem. Soc.* **2016**, *138*, 2528.
[19] K. Rakstys, A. Abate, M. I. Dar, P. Gao, V. Jankauskas, G. Jacopin, E. Kamarauskas, S. Kazim, S. Ahmad, M. Grätzel, M. K. Nazeeruddin, *J. Am. Chem. Soc.* **2015**, *137*, 16172.
[20] H. Nishimura, N. Ishida, A. Shimazaki, A. Wakamiya, A. Saeki, L. T. Scott, Y. Murata, *J. Am. Chem. Soc.* **2015**, *137*, 15656.
[21] A. Molina-Ontoria, I. Zimmermann, I. Garcia-Benito, P. Gratia, C. Roldán-Carmona, S. Aghazada, M. Grätzel, M. K. Nazeeruddin, N. Martín, *Angew. Chem. Int. Ed.* **2016**, *55*, 6270.
[22] X. Yin, L. Guan, J. Yu, D. Zhao, C. Wang, N. Shrestha, Y. Han, Q. An, J. Zhou, B. Zhou, Y. Yu, C. R. Grice, R. A. Awni, F. Zhang, J. Wang, R. J. Ellingson, Y. Yan, W. Tang, *Nano Energy* **2017**, *32*, 163.
[23] X. Liu, F. Kong, R. Ghadari, S. Jin, T. Yu, T. Yu, W. Chen, G. Liu, Z. Tan, J. Chen, *Chem. Commun.* **2017**, *53,* 9558.
[24] Y.-D. Lin, B.-Y. Ke, K.-M. Lee, S. H. Chang, K.-H. Wang, S. H. Huang, C.-G. Wu, P. -T, Chou, S. Jhulki, J. N. Moorthy, Y. J. Chang, K.-L. Liau, H.-C. Chung, C.-Y. Liu, S.-S. Sun, T. J. Chow, *ChemSusChem* **2016**, *9,* 274.
[25] J. Zhang, B. Xu, M. B. Johansson, M. Hadadian, J. P. C. Baena, P. Liu, Y. Hua, N. Vlachopoulos, E. M. J. Johansson, G. Boschloo, L. Sun, A. Hagfeldt, *Adv. Energy Mater.* **2016**, *6*, 1502536.
[26] A. Krishna, A. C. Grimsdale, *J. Mater. Chem. A* **2017**, *5*, 16446.
[27] J. Zhang, B. Xu, L. Yang, C. Ruan, L. Wang, P. Liu, W. Zhang, N. Vlachopoulos, L. Kloo, G. Boschloo, L. Sun, A. Hagfeldt, E. M. J. Johansson, *Adv. Energy Mater.* **2017**, 1701209.
[28] P. Kumaresan, S. Vegiraju, Y. Ezhumalai, S. L. Yau, C. Kim, W.-H. Lee, M.-C. Chen, *Polymer* **2014**, *6*, 2645.
[29] P. J. L. Bredas, J. P. Calbert, D. A. da Silva Filho, J. Cornil, *Proc. Natl. Acad. Sci. USA.* **2002**, *99*, 5804.
[30] R. P. Ortiz, A. Facchetti, T. J. Marks, J. Casado, M. Z. Zgierski, M. Kozaki, V. Hernández, J. T. L. Navarrete, *Adv. Funct. Mater.* **2009**, *19*, 386.
[31] Z. Fei, X. Gao, J. Smith, P. Pattanasattayavong, E. B. Domingo, N. Stingelin, S. E. Watkins, T. D. Anthopoulos, R. J. Kline, M. Heeney, *Chem. Mater.* **2013**, *25*, 59.
[32] M. Zhang, Y. Wang, M. Xu, W. Ma, R. Li, P. Wang, *Energy Environ. Sci.* **2013**, *6*, 2944.
[33] M. Franckevicius, A. Mishra, F. Kreuzer, J. Luo, S. M. Zakeeruddin, M. Grätzel, *Mater. Horiz.* **2015**, *2*, 613.
[34] S. Ma, H. Zhang, N. Zhao, Y. Cheng, M. Wang, Y. Shen, G. Tu, *J. Mater. Chem. A* **2015**, *3*, 12139.
[35] S. Paek, I. Zimmermann, P. Gao, P. Gratia, K. Rakstys, G. Grancini, M. K. Nazeeruddin, M. A. Rub, S. A. Kosa, K. A. Alamry, A. M. Asiri, *Chem. Sci.* **2016**, *7*, 6068.
[36] Y. Sun, G. C. Welch, W. L. Leong, C. J. Takacs, G. C. Bazan, A. J. Heeger, *Nat. Mater.* **2012**, *11*, 44.
[37] B. Xu, E. Sheibani, P. Liu, J. Zhang, H. Tian, N. Vlachopoulos, G. Boschloo, L. Kloo, A. Hagfeldt, L. Sun, *Adv. Mater.* **2014**, *26*, 6629.

[38] Y. Xu, J. Shi, S. Lv, L. Zhu, J. Dong, H. Wu, Y. Xiao, Y. Luo, S. Wang, D. Li, X. Li, Q. Meng, *ACS Appl. Mater. Interfaces* **2014**, *6*, 5651.
[39] J. Zhang, B. Xu, M. B. Johansson, N. Vlachopoulos, G. Boschloo, L. Sun, E. M. J. Johansson, A. Hagfeldt, *ACS Nano* **2016**, *10*, 6816.
[40] L. Zheng, Y.-H. Chung, Y. Ma, L. Zhang, L. Xiao, Z. Chen, S. Wang, B. Qu, Q. Gong, *Chem. Commun.* **2014**, *50*, 11196.
[41] D. W. Zhao, P. Liu, X. W. Sun, S. T. Tan, L. Ke, A. K. K. Kyaw, *Appl. Phys. Lett.* **2009**, *95*, 153304.
[42] L. M. Chen, Z. Xu, Z. R. Hon, Y. Yang, *J. Mater. Chem.* **2010**, *20*, 2575.
[43] Y. X. Zhao, A. M. Nardes, K. Zhu, *Appl. Phys. Lett.*, **2014**, *104*, 213906.
[44] F. Giordano, A. Abate, J. P. Correa Baena, M. Saliba, T. Matsui, S. H. Im, S. M. Zakeeruddin, M. K. Nazeeruddin, A. Hagfeldt, M. Grätzel, *Nat. Commun.* **2016**, *7*, 10379.
[45] T. Lei, Y. Cao, X. Zhou, Y. Peng, J. Bian, J. Pei, *Chem. Mater.* **2012**, *24*, 1762.
[46] M. Li, Z.-K. Wang, Y.-G. Yang, Y. Hu, S.-L. Feng, J.-M. Wang, X.-Y. Gao, L.-S. Liao, *Adv. Energy Mater.* **2016**, *6*, 1601156

Manuscript received: October 16, 2018
Revised manuscript received: November 1, 2018
Accepted manuscript online: November 7, 2018
Version of record online: January 15, 2019

